Real-Time Tracking and In Vivo Visualization of β-Galactosidase Activity in Colorectal Tumor with a Ratiometric NIR Fluorescent Probe

Kaizhi Gu,[†,§] Yisheng Xu,[‡,§] Hui Li,[#,§] Zhiqian Guo,[*,†] Shaojia Zhu,[⊥] Shiqin Zhu,[†] Ping Shi,[⊥] Tony D. James,[Δ] He Tian,[†] and Wei-Hong Zhu[*,†]

[†]Key Laboratory for Advanced Materials and Institute of Fine Chemicals, Shanghai Key Laboratory of Functional Materials Chemistry, School of Chemistry and Molecular Engineering, East China University of Science and Technology, Shanghai 200237, China.

[‡]State Key Laboratory of Chemical Engineering, East China University of Science and Technology, Shanghai 200237, China.

[#] Department of Radiology, Shanghai Jao Tong University Affiliated Sixth People's Hospital, Shanghai 200233, China

[⊥]State Key Laboratory of Bioreactor Engineering, East China University of Science and Technology, Shanghai 200237, China

[Δ]Department of Chemistry, University of Bath, Bath BA2 7AY, United Kingdom.

E-mail: whzhu@ecust.edu.cn; guozq@ecust.edu.cn

ABSTRACT: Development of "smart" noninvasive bioimaging probes for trapping specific enzyme activities is highly desirable for cancer therapy *in vivo*. Given that β-galactosidase (β-gal) is an important biomarker for cell senescence and primary ovarian cancers, we design an enzyme-activatable ratiometric near-infrared (NIR) probe (DCM-βgal) for the real-time fluorescent quantification and trapping of β-gal activity *in vivo* and *in situ*. DCM-βgal manifests significantly ratiometric and turn-on NIR fluorescent signals simultaneously in response to β-gal concentration, which make it favorable for monitoring dynamic β-gal activity *in vivo* with self-calibration in fluorescent mode. We exemplify DCM-βgal for the ratiometric tracking of endogenously overexpressed β-gal distribution in living 293T cells *via* the *lacZ* gene transfection method and OVCAR-3 cells, and further realize real-time *in vivo* bioimaging of β-gal activity in colorectal tumor-bearing nude mice. Advantages of our system include light-up ratiometric NIR fluorescence with large Stokes-shift, high photo-stability, and displays pH independency under the physiological range, allowing for the *in vivo* real-time evaluation of β-gal activity at the tumor site with high-resolution three-dimensional bioimaging for the first time. Our work provides a potential tool for *in vivo* real-time tracking enzyme activity in preclinical applications.

KEYWORDS: Fluorescent probe, near-infrared, ratiometric tracking, β-galactosidase, enzyme activity

INTRODUCTION

Molecular bioimaging of enzyme activity *in vivo* is rapidly emerging as a powerful strategy for accurate disease diagnostics.[1-6] The development of "smart" noninvasive imaging reagents for the determination of specific enzyme activity *in vivo* is critically required for cancer diagnosis.[7-15] However, during the onset and progression of cancer, the dynamic living system complexity makes it difficult to track and visualize *in vivo* enzyme activity. As a typical enzyme, β-galactosidase (β-gal) has been demonstrated as an important biomarker for cell senescence and primary ovarian cancers.[16-19] Much effort has been devoted to treating β-gal as an enzymatic target with fluorescent probes to visualize its activity in preclinical diagnosis.[20-25] However, owing to the limited indirect prediction *via* histology or *in vitro* experiments, the currently fluorescent β-gal probes are not capable of precisely tracking *in vivo* real-time enzyme activity required for cancer diagnosis.

One of the major obstacles encountered with fluorescence imaging of enzyme activity *in vivo* is the strong intrinsic auto-fluorescence background from living tissues, which significantly compromises the accuracy of measurement under physiological conditions. Near-infrared (NIR) fluorescence imaging is an accessible tool for noninvasive *in vivo* visualization of mammalian tissues with decreased auto-fluorescence, low light scattering and high penetration depth.[26-34] Weissleder *et al.* designed DDAOG emitting in the NIR region for *in vivo* detection of β-gal activity,[35] but severe cross-talk between the excitation and emission spectra weakening the ability to capture valid signals. Moreover, in contrast with the single wavelength fluorescence-intensity based systems, ratiometric fluorescence probes are of considerable practical

advantage due to enhanced signal-to-background ratio, in which the detectable ratio signal can be obtained by two independent read-out channels of activated *versus* unreacted probes resulting in improved and reliable signal quantification.[36-40]

Scheme 1. Proposed Sensing Mechanism for β-Gal Enzymatic Activation of DCM-βgal.

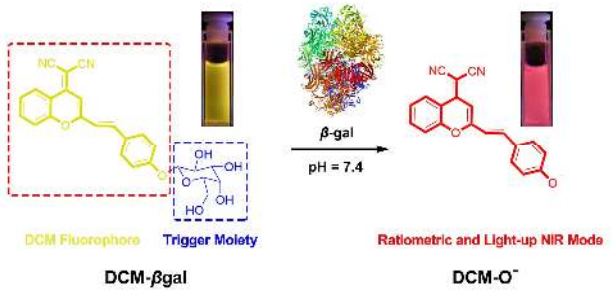

The aforementioned concerns encourage us to create a novel fluorescent probe for tracking the *in vivo* behavior of the important β-gal enzyme and clarifying its potential role in tumor diagnosis. Our strategy is based on grafting an enzyme-active trigger onto a controllable emissive, bright and photostable NIR chromophore. Controllable emission with large spectral shifts *via* modulation of the electron donor ability of novel NIR-active fluorophores is critical and required for excellent imaging contrast agents. Herein, we report on a β-gal-targeting ratiometric and light-up NIR fluorescent probe (DCM-βgal, Scheme 1), in which the dicyanomethylene-4*H*-pyran (DCM) chromophore is utilized as a NIR fluorescence reporter,[41-45] and a β-gal cleavable unit as the enzyme-active trigger. As expected, the emission wavelength is distinctly changed upon removal of the β-gal-responsive group (the enzyme-triggered moiety, Scheme 1), resulting in a new broad emission band in the NIR region. The system enables the direct and accurate monitoring of intracellular endogenous β-gal distribution in transfection living cells with a high signal-to-noise ratio. That in turn allows for real-time *in vivo* bioimaging of β-gal activity in colorectal tumor-bearing nude mice. Probe DCM-βgal possesses several striking characteristics, such as ratiometric fluorescence activation with a light-up NIR emission and high photo-stability in physiological range. To the best of our knowledge, DCM-βgal is the first light-up NIR fluorescence probe for the *in vivo* and *in situ* tracking β-gal activity in tumor-bearing nude mice using high-resolution three-dimensional fluorescence imaging.

RESULTS AND DISCUSSION

Design and Synthesis. NIR-active fluorophores are favored for *in vivo* optical imaging contrasts. As well-known laser dyes, DCM derivatives could perform controllable emission in the NIR region with large spectral shifts *via* tuning electron donor ability,[41-46] which offer such critical features as excellent imaging contrasts. Specifically, DCM-OH has favorable donor–π–acceptor (D–π–A) characteristics for sensor design, with a phenolic group for regulating electron donating capability. The emission wavelength could be distinctly changed upon removing the substituted group (for instance, the enzyme-triggered moiety, Scheme 1). In this regard, we designed probe DCM-βgal by grafting a β-gal activatable unit onto DCM-OH moiety. The synthetic route for the probe was depicted in the Supporting Information (SI). DCM-βgal was finally synthesized with a yield of 33% under mild conditions, which was fully characterized by ^{1}H and ^{13}C NMR, and HRMS (SI).

Spectroscopic Properties and Optical Response to β-Gal. To test the validity of this probe, the spectral properties of DCM-βgal were investigated with β-gal in physiological buffer solution. DCM-βgal shows a typical broad absorption band at 440 nm from its intrinsic intramolecular charge transfer (ICT). Upon titration with 12 U β-gal, the absorption peak of DCM-βgal at 440 nm decreased, and a concomitant new absorption peak appeared at about 535 nm (Figure 1A), which is in perfect accordance with the absorption of DCM-O$^-$ (Figures S1 and S2 in SI). The well-defined isosbestic point at 450 nm clearly demonstrates the coexistence of DCM-βgal and the cleavage product (DCM-O$^-$). The color change from faint yellow to rose red allows the colorimetric detection of β-gal using the naked eye, which is invoked by a large red shift of *ca.* 100 nm in the absorption spectra.

As expected, the emission profiles of DCM-βgal are correlated to those of the absorption profiles in the presence of β-gal. When excited at the isosbestic point of 450 nm, an obvious ratiometric fluorescent signal ($I_{685\ nm}/I_{500\ nm}$) was observed. As shown in Figure 1B, a new broad band falling into the emission range of 550-800 nm sharply increased, along with a decrease in the emission band at 500 nm. Upon excitation of the new absorption peak at 535 nm, a remarkable NIR fluorescence enhancement was observed with a peak at 685 nm (Figure 1C and Table S1 in SI). Clearly, the new distinct large red-shift fluorescence response confirms that β-gal-mediated hydrolysis of DCM-βgal liberates the oxygen atom as a strong electron donor in the D–π–A structure, thereby increasing ICT and shifting the emission maximum to the NIR region.

Figure 1D depicts the ratiometric fluorescent signal ($I_{685\ nm}/I_{500\ nm}$) as a function of time. It takes about 35 min to reach a plateau, which is also directly reflected by the fluorescence response at 685 nm (Figure S3 in SI). The kinetic results imply that the fluorescent response can be utilized for the rapid detection of β-gal, which is much faster than that of previously reported FDG (3 h).[47] Therefore, in our subsequent experimental assays, the detection limit was set at 35 min. Specifically, when the probe was incubated with 12 U β-gal for *ca.* 35 min, a 14-fold increase was observed in the fluorescence ratio of $I_{685\ nm}/I_{500\ nm}$ (Figure 1B), or a 34-fold fluorescence enhancement at 685 nm was observed (Figure 1C). Notably, the plot of the $I_{685\ nm}/I_{500\ nm}$ ratio or $I_{685\ nm}$ against the concentrations of β-gal ranging from 0 to 12 U both display a good linear relationship (Inset of Figures 1B and 1C). Hence, the linear curve of the $I_{685\ nm}/I_{500\ nm}$ ratio allows for

the convenient quantitative detection of β-gal very convenient over this concentration range. The Michaelis constant (K_m) of DCM-βgal in the β-gal-catalyzed reaction was calculated to be 60.1 μM (Table S2 in SI), which was much lower than that of commercial *X*-gal (260.6 μM). Obviously, DCM-βgal shows higher affinity to β-gal than *X*-gal. Furthermore, derived from the change in concentration-dependent ratio, the detection limit of DCM-βgal was calculated as 1.7×10^{-4} U mL^{-1}, indicative of ultra-sensitivity to changes in β-gal expression (Figure S4 in SI). Consequently, DCM-βgal enables the fast and quantitative ratiometric fluorescence detection of β-gal.

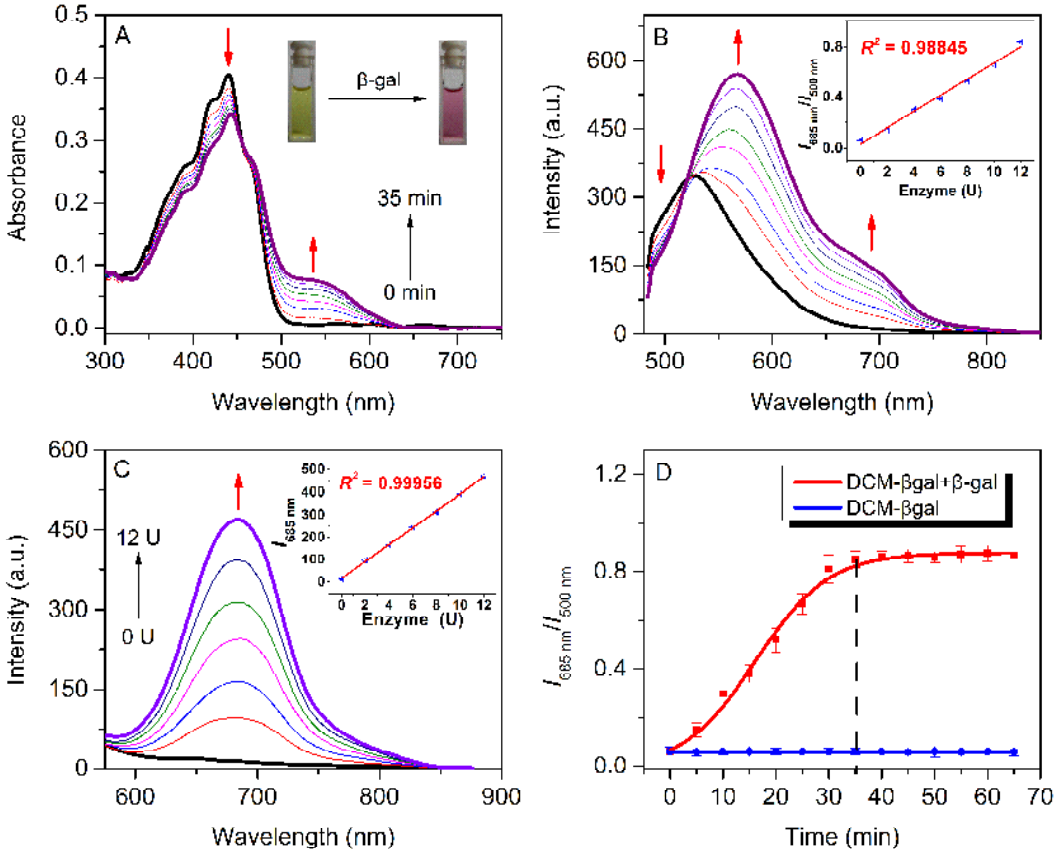

Figure 1. Spectral profiles of DCM-βgal (10 μM) incubation with β-gal (12 U) in aqueous solution (PBS/DMSO = 7:3, v:v, pH = 7.4, 37 °C): (A) Time dependence of absorption spectra. Inset: images before and after treatment with β-gal; (B) Time dependence of emission spectra (0-35 min), λ_{ex} = 450 nm. Inset: the relationship between $I_{685\,nm}/I_{500\,nm}$ and β-gal concentration; (C) Emission spectra of DCM-βgal upon addition of β-gal (0-12 U), λ_{ex} = 535 nm. Inset: the relationship between $I_{685\,nm}$ and β-gal concentration; (D) Time dependence of $I_{685\,nm}/I_{500\,nm}$ for DCM-βgal in the presence (red) and absence (blue) of β-gal, λ_{ex} = 450 nm.

Sensing Mechanism. For taking insight into the activation of DCM-βgal with enzyme, a series of experiments were also carried out. The HPLC results confirmed that DCM-βgal is a substrate of β-gal, which exclusively generates DCM-O$^-$ (Figure S5 in SI). In the ESI-MS spectra of DCM-βgal with β-gal, the peaks of DCM-βgal and DCM-O$^-$ were found at *m/z* 497.1441 and 311.0697 (Figure S6 in SI), respectively. In fact, the aforementioned spectra from the reaction of DCM-βgal with β-gal resemble those of DCM-O$^-$, which also strongly supports the fact that the enzyme-triggered cleavage reaction causes the release of free DCM-O$^-$. All these observations confirm that DCM-βgal can be hydrolyzed by breaking the C-O bond upon enzyme-reactive reaction with β-gal to release an electron-rich aglycon, DCM-O$^-$, which emits in the NIR region and possesses a distinct ratiometric fluorescent signal with a large spectral shift.

To test the interference with other biological analytes, the reactivity of DCM-βgal towards a variety of enzyme species, amino acids and biomolecules was examined. There were only subtle changes in fluorescence ratio upon the addition of 100 equiv of cellulase, reductase, lysozyme, esterase, cysteine, homocysteine, glutathione, dithiothreitol, hydrogen peroxide and hydrogen sulfide. However, only when treated with β-gal was the large and distinct enhancement of fluorescence ratio ($I_{685\,nm}/I_{500\,nm}$) observed (Figure 2A), accompanying by an obvious color change from faint yellow to rose red (Figure 2B), which corresponds to the evolution of DCM-O$^-$. These results demonstrate the excellent selectivity of DCM-βgal towards β-gal over other competitive analytes, which is required in

order to achieve accurate detection under practical applications.

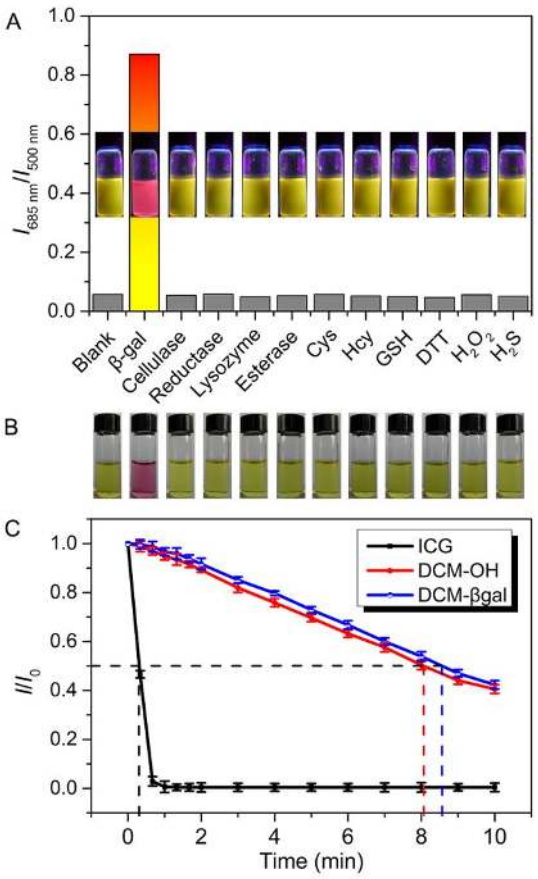

Figure 2. (A) Fluorescence ratio ($I_{685\,nm}/I_{500\,nm}$) responses and (B) color changes of DCM-βgal (10 μM) to various analytes in aqueous system (PBS/DMSO = 7:3, v:v; pH = 7.4, 37 °C). Bars correspond to the fluorescence ratio ($I_{685\,nm}/I_{500\,nm}$) of DCM-βgal with 100 equivalent of analytes, λ_{ex} = 450 nm. (C) Time-dependent fluorescence intensity of ICG (10 μM, monitored at 812 nm, and λ_{ex} = 780 nm), DCM-OH (10 μM, monitored at 565 nm, and λ_{ex} = 450 nm), and DCM-βgal (10 μM, monitored at 525 nm, and λ_{ex} = 450 nm) under sustained illumination.

Photo-Stability. The high photo-stability of DCM-βgal and DCM-OH is highly desirable to perform long time *in vivo* tracking enzyme activity in preclinical applications. Here the photo-stability of DCM-βgal and DCM-OH was evaluated by time-course fluorescence measurements upon sustained illumination in aqueous solution. The commercially FDA-approved NIR dye ICG was chosen as a control. After exposure to high density light (Hamamatsu, LC8 Lightningcure, 300 W) for about 60 s, the fluorescence intensity of ICG was reduced to a minimum value, indicating that ICG was almost completely decomposed, however, 90% of the DCM-βgal and DCM-OH fluorescence intensity remained under the same conditions. Indeed, the fluorescence half-life of the DCM-βgal was 35-fold longer than that of ICG (Figure 2C). The photo-stability of both DCM-βgal and DCM-OH is much better than ICG, which is a critical factor for the long time tracking and bioimaging *in vivo*.

pH Profiles of DCM-βgal and DCM-OH. pH is an important factor on the photophysical properties of the sensing probe. We subsequently evaluated the pH dependence of the emission profiles of DCM-OH and DCM-βgal (Figure S7 in SI). There was negligible fluorescence change at 685 nm for DCM-βgal during the pH range from 3.5 to 9.8 upon excitation at 535 nm. Obviously, the fluorescence of DCM-βgal remains silent over the physiological pH range. More excitingly, the hydrolytic product of DCM-βgal can only be produced at the optimal physiological pH range. That is, the pK_a of DCM-OH was measured to be *ca.* 7.1which allows DCM-βgal to favorably exploit the physiological conditions of living systems.

Ratiometric Imaging of Endogenous β-Gal in Living Cells. We further explored whether DCM-βgal could be used for the ratiometric tracking and imaging of endogenous β-gal activity in living cells. As a high efficient and facile transfection process, human embryonic kidney cells (293T cells) were chosen as model cell lines. In order to generate endogenous β-gal in living cells, *lacZ* gene was introduced into 293T cells by employing a gene transfection method to overexpress β-gal. The MTT assay results indicate that both DCM-βgal and its hydrolysate DCM-OH have minimal toxicity and enjoy superior biocompatibility toward cultured cell lines (Figure S8 in SI). After incubation with DCM-βgal (10 μM) at 37 °C for 30 min, the *lacZ*-(-) 293T cells without overexpressed β-gal exhibited both bright fluorescence in green channel and little fluorescence in the red channel (Figures 3B and 3C), which corresponds to the two peaks (525 and 685 nm) in the emission spectra of DCM-βgal. In contrast, the *lacZ*-(+) 293T cells with overexpressed β-gal exhibited a decreased fluorescence in green channel, and an concomitant increase in the red channel (Figures 3I and 3J), corresponding to formation of DCM-O$^-$. The ratiometric imaging of endogenous β-gal activity was constructed from red and green channels (F_{red}/F_{green}, Figures 3D and 3K). The average emission ratio F_{red}/F_{green} of the *lacZ*-(-) and *lacZ*-(+) 293T cells was calculated to be 0.43 and 2.20, respectively. An approximate 5-fold increase in ratio for the *lacZ*-(+) compared to *lacZ*-(-) 293T cells was observed (Figure S8 in SI). Therefore, we have successfully demonstrated the quantitative ratiometric imaging of endogenous β-gal activity.

Moreover, upon excitation at 560 nm, a clear fluorescence image was captured in the overexpressed *lacZ*-(+) 293T cells in the NIR region due to the liberation of DCM-O$^-$ by intracellular β-gal, while a fluorescent signal was barely observed for the *lacZ*-(-) 293T cells (Figures 3F and 3M). Moreover, OVCAR-3 from human ovarian cancer patients that has been demonstrated overexpression of endogenous β-gal[19,25,48] was also chosen as another cell lines model. As expected, the same as in living 293T cells via the *lacZ* gene transfection method, we also clearly observed the quantitative ratiometric and light-up NIR

imaging of endogenous β-gal activity in OVCAR-3 cells (Figures 3O-3U). As shown in Figure 3A1, the light-up fluorescence signals were sharply decreased in the presence of a competitive β-gal inhibitor (D-galactose)[49]. These results further confirmed that DCM-βgal could monitor endogenous β-gal activity. Notably, since the incubation of DCM-βgal was processed without any other complex loading techniques, DCM-βgal has been demonstrated to be highly cell membrane-permeable and photo-stable. These results suggested that DCM-βgal can be specifically activated in β-gal-expressing cells, thereby providing a ratiometric and light-up NIR readout for the *in situ* quantitative tracking and visualization of endogenous β-gal activity in living cells.

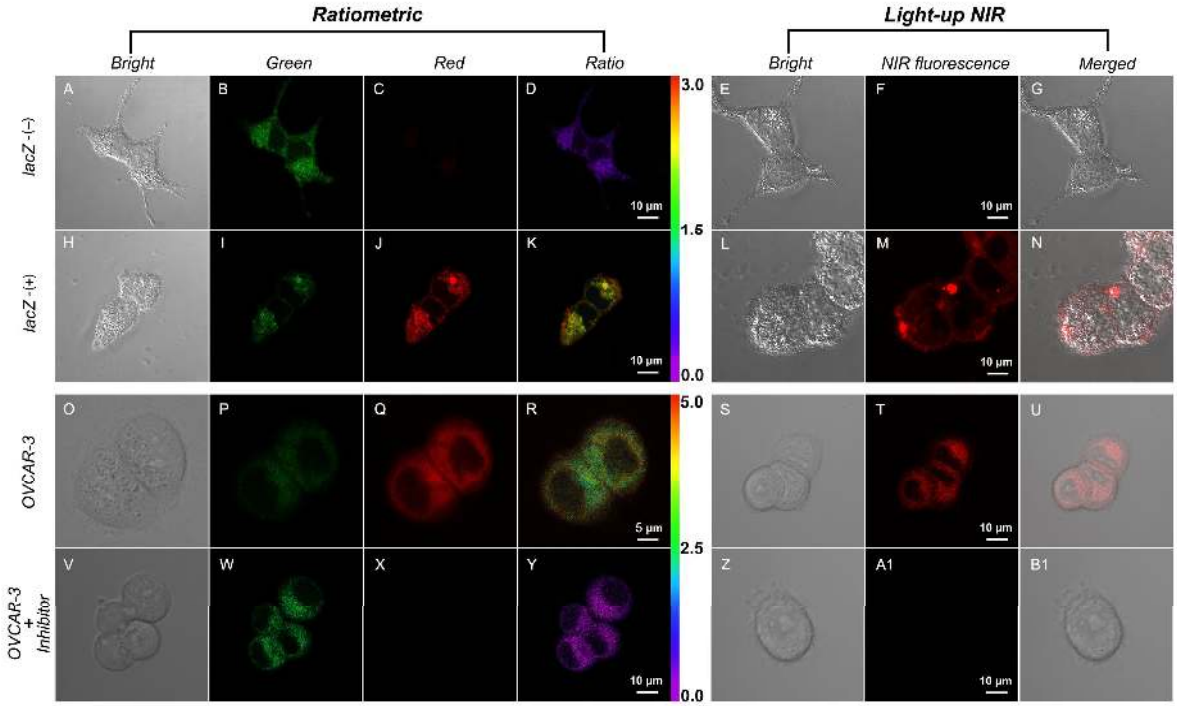

Figure 3. Confocal and ratiometric images of 293T and OVCAR-3 cells incubated with DCM-βgal (10 μM) for 30 min: (A-G) *lacZ*-(-) 293T cells without overexpressed β-gal, (H-N) *lacZ*-(+) 293T cells with overexpressed β-gal, (O-U) OVCAR-3 cells, and (V-B1) OVCAR-3 cells pretreated with inhibitor for 30 min. Green channel obtained from 490-530 nm, red channel obtained from 650-720 nm, and ratiometric images generated from red and green channel, λ_{ex} = 404 nm. NIR fluorescence images obtained from 605-725 nm, λ_{ex} = 560 nm. The ratiometric images were obtained by the image analysis software, Image Pro-plus 6.0.

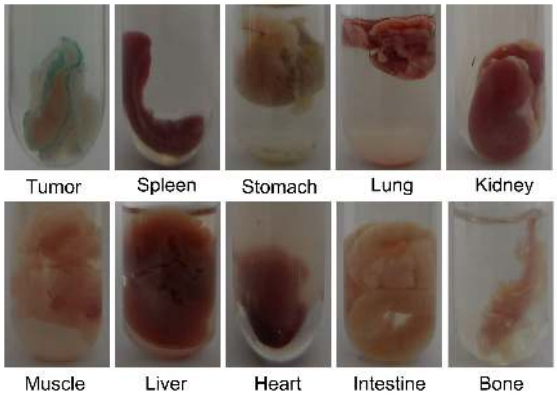

Figure 4. Biodistribution of avidin-β-gal targeting to LoVo tumor-bearing mice *in vivo*. Avidin-β-gal (100 μg) in PBS was intravenously injected into LoVo-implanted mice, and the mouse was sacrificed after 18 h. The main internal organs (tumor, spleen, stomach, lung, kidney, muscle, liver, heart, intestine, and bone) were removed and stained with *X*-gal (0.04 mg mL^{-1}) for another 2.5 h.

Real-time *in vivo* Imaging of β-Gal Activity in Tumors. The current fluorescent probes for imaging of β-gal activity are not very suitable for *in vivo* experiments because their emissions are not located in NIR region,[20-23] and thus fail to penetrate deeper tissue and are complicated by intrinsic auto-fluorescence background signals. Recently, Urano *et al*. have made important progress by developing HMRef-βGal for *in vivo* fluorescence endoscopy of β-gal activity.[25] Inspired by the distinct "light-up" NIR emission, we next examined its capability for real-time *in vivo* visualization of β-gal activity in tumors. A commercial tumor targeting reagent (avidin-β-gal) was initially applied to localize β-gal to tumor growth of human colorectal cancer LoVo cell xenografts *in vivo* by intravenous injection[50,51] since avidin has high affinity for lectins on the surface of LoVo cells.[52,53] We next examined whether avidin-β-gal could be targeted to tumor

cells *in vivo* by intravenous injection. After injection for 18 h, the main internal organs were obtained by anatomy and stained with *X*-gal (0.04 mg mL^{-1}), a commercial detection reagent for β-gal. After incubation for another 2.5 h, only in the disseminated tumor was a blue precipitate observed, suggesting that avidin-β-gal can be efficiently targeted to LoVo tumor cells *in vivo* without loss of the enzymatic activity (Figure 4). The mice bearing subcutaneously implanted tumors were administered DCM-βgal by intravenous or intratumoral injection, and then scanned at different time points with an IVIS Lumina Kinetic Series III imaging system.

Owing to amplified fluorescence signals by enzymatic turnover and particular low background interference in NIR region, the remarkable NIR fluorescent signal was observed in the tumor site after *in situ* injection of DCM-βgal (0.0375 mg kg^{-1}, Figure 5A) for β-gal upregulating mice induced by intravenous injection of avidin-β-gal (100 μg). It should be noted that after merely 5 min post injection, the NIR fluorescence signal was already clearly appreciated in tumor, indicative of the rapid activation of DCM-βgal and the fluorescence intensity gradually increased and reached a maximum level after 3 h post injection, then slowly decayed as the time increased. In comparison, for the unpretreated tumor-bearing mouse, there is minimal light-up fluorescence under the same conditions (Figure 5B). To further confirm that the NIR fluorescent signal comes from the cleavage of DCM-βgal by β-gal in the tumor, we also recorded the *ex vivo* fluorescence images of tumor and other normal organs collected immediately after sacrificing the mice with upregulating β-gal at 3 h post injection. In consistent with the *in vivo* results, only the tumor was fluorescent (Figure 5C). As expected, the fluorescence images of other normal organs and tumor gained from the control mice displayed no fluorescence signal (Figure 5D).

Real-time three-dimensional imaging is a powerful tool for accurate disease diagnostics, particular for suspicious lesions with high spatiotemporal precision. The preferable characteristics of DCM-βgal with light-up NIR performance and rapid response to β-gal activity (5 min) at the lesion site make it suitable to perform real-time three-dimensional imaging. After post-injection of the probe into the mice containing abundant β-gal, we obtained the real-time high-resolution three-dimensional fluorescence image with an IVIS Spectrum CT imaging system. Observed from different perspective in real time, the tumor site was precisely located *in vivo* and *in situ* with the help of NIR light-up fluorescence signals (Figure 5E and Movie 1 in SI). By contrast, in the control experiments, there was no fluorescence signal located in tumors (Figure S10 and Movie 2 in SI). For the first time, we exemplify the *in situ* three-dimensional fluorescence imaging to visualize real-time *in vivo* β-gal activity in tumors.

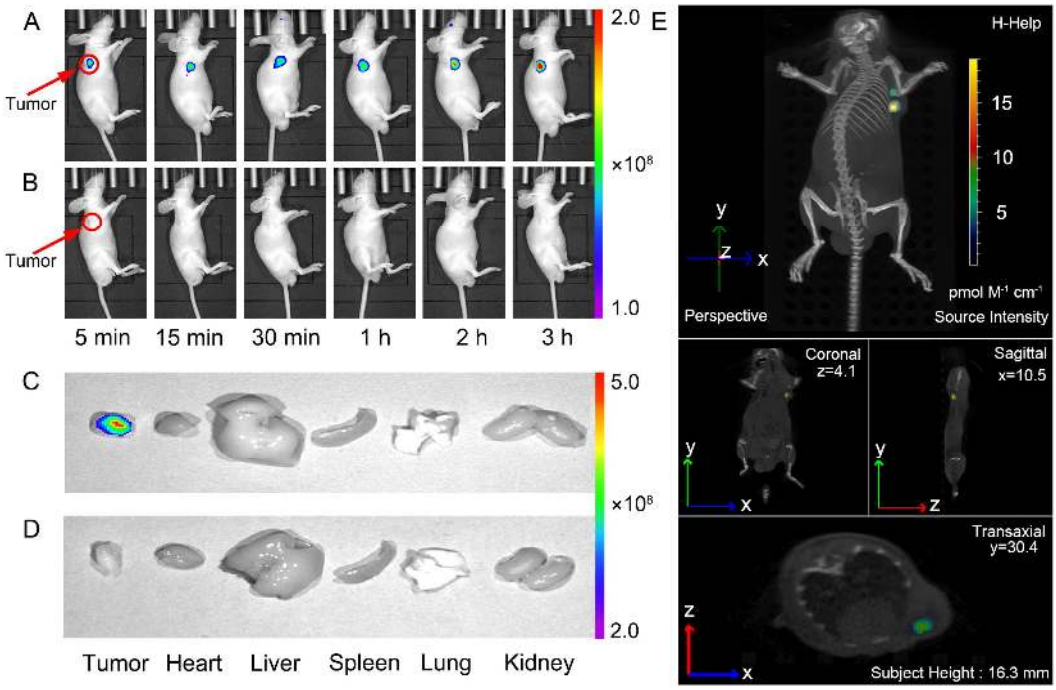

Figure 5 (A and B) *In vivo* imaging of β-gal activity in tumor-bearing nude mice after tumor-injection, (C and D) fluorescence images of the main internal organs after anatomy, and (E) three-dimensional *in vivo* imaging of β-gal activity in tumor-bearing nude mice after tumor-injection of DCM-βgal for 3 h: (A, C and E) avidin-β-gal (100 μg) in PBS was intravenously injected into LoVo-implanted mice, and after 18 h DCM-βgal was then injected into the mice, (B and D) tumor-bearing mice were not pretreated with avidin-β-gal before injection of DCM-βgal acting as the control.

CONCLUSIONS

We have developed a ratiometric and light-up NIR fluorescent probe DCM-βgal, composed of the DCM scaffold as a typical NIR fluorescence reporter and a β-gal cleavable unit as the enzyme-active trigger. The probe has higher photo-stability than commercial ICG, and displays pH independency over the physiological range. DCM-βgal displays higher affinity for β-gal than commercial *X*-gal and much faster response to β-gal than the previously reported FDG. More importantly, this probe was successfully applied for *in situ* and *in vivo* visualization of β-gal activity in human colorectal tumor in mice model, as well as real-time trapping of intracellular endogenous β-gal distribution in over-expressed living 293T cells *via* the *lacZ* gene transfection method. For the first time *in vivo* real-time capture of β-gal activity at tumor site with high-resolution three-dimensional view was performed. In light of its simplicity, sensitivity and biocompatibility, this ratiometric and light-up enzyme-activatable NIR fluorescent probe provides an accessible tool for the unprecedented quantification and trapping of β-gal activity *in vivo* for human colorectal cancer diagnosis.

ASSOCIATED CONTENT

More detailed experimental procedures, characterizations, supplementary optical spectra and figures can be found in Supporting Information. This material is available free of charge via the Internet at http://pubs.acs.org.

AUTHOR INFORMATION

Corresponding Author

whzhu@ecust.edu.cn; guozq@ecust.edu.cn;

Author Contributions

§K.G., Y.X. and H.L. contributed equally.

Notes

The authors declare no competing financial interest.

ACKNOWLEDGMENTS

This work was supported by National 973 Program (2013CB733700), NSFC for Creative Research Groups (21421004) and Distinguished Young Scholars (21325625), NSFC/China, Oriental Scholarship, Scientific Committee of Shanghai (14ZR1409700 and 15XD1501400), Shanghai Pujiang Program (13PJD010), Fok Ying Tong Education Foundation (142014), the Fundamental Research Funds for the Central Universities (WK1013002 and 22220131310), and Programme of Introducing Talents of Discipline to Universities (B16017). The Catalysis And Sensing for our Environment (CASE) network is thanked for research exchange opportunities. T.D.J. thanks ECUST for a guest professorship.

REFERENCES

(1) Weissleder, R.; Pittet, M. J. *Nature* **2008**, *452*, 580-589.
(2) Razgulin, A.; Ma, N.; Rao, J. *Chem. Soc. Rev.* **2011**, *40*, 4186-4216.
(3) You, L.; Zha, D.; Anslyn, E. V. *Chem. Rev.* **2015**, *115*, 7840–7892.
(4) Lee, M. H.; Kim, J. S.; Sessler, J. L. *Chem. Soc. Rev.* **2015**, *44*, 4185-4191.
(5) Talukder, P.; Chen, S. X.; Roy, B.; Yakovchuk, P.; Spiering, M. M.; Alam, M. P.; Madathil, M. M.; Bhattacharya, C.; Benkovic, S. J.; Hecht, S. M. *Biochemistry* **2015**, *54*, 7457–7469.
(6) Tang, J.; Sheng, Y.; Hu, H.; Shen, Y. *Prog. Polym. Sci.* **2013**, *38*, 462-502.
(7) Xu, Q.; Heo, C. H.; Kim, G.; Lee, H. W.; Kim, H. M.; Yoon, J. *Angew. Chem. Int. Ed.* **2015**, *54*, 4890-4894.
(8) Burke, H. M.; Gunnlaugsson, T.; Scanlan, E. M.; *Chem. Commun.* **2015**, *51*, 10576-10588.
(9) Li, Y.; Sun, Y.; Li, J.; Su, Q.; Yuan, W.; Dai, Y.; Han, C.; Wang, Q.; Feng, W.; Li, F. *J. Am. Chem. Soc.* **2015**, *137*, 6407-6416.
(10) Wang, F.; Zhu, Y.; Zhou, L.; Pan, L.; Cui, Z.; Fei, Q.; Luo, S.; Pan, D.; Huang, Q.; Wang, R.; Zhao, C.; Tian, H.; Fan, C. *Angew. Chem. Int. Ed.* **2015**, *54*, 7349-7353.
(11) Bhuniya, S.; Maiti, S.; Kim, E.; Lee, H.; Sessler, J. L.; Hong, K. S.; Kim, J. S. *Angew. Chem. Int. Ed.* **2014**, *53*, 4469-4474.
(12) Zhou, Z.; Ma, X.; Murphy, C. J.; Jin, E.; Sun, Q.; Shen, Y.; Van Kirk, E. A.; Murdoch, W. J. *Angew. Chem. Int. Ed.* **2014**, 53, 10949-10955.
(13) Kim, E.; Bhuniya, S.; Lee, H.; Kim, H. M.; Cheong, C.; Maiti, S.; Hong, K. S.; Kim, J. S. *J. Am. Chem. Soc.* **2014**, *136*, 13888-13894.
(14) Xuan, W.; Sheng, C.; Cao, Y.; He, W.; Wang, W. *Angew. Chem. Int. Ed.* **2012**, *51*, 2282-2284.
(15) Zamora-Olivares, D.; Kaoud, T. S.; Jose, J.; Ellington, A.; Dalby, K. N.; Anslyn, E. V. *Angew. Chem. Int. Ed.* **2014**, *53*, 14064 –14068.
(16) Spergel, D. J.; Krüth, U.; Shimshek, D. R.; Sprengel, R.; Seeburg, P. H. *Prog. Neurobiol.* **2001**, *63*, 673-686.
(17) Alam, J.; Cook, J. L. *Anal. Biochem.* **1990**, *188*, 245-254.
(18) Dimri, G. P.; Lee, X.; Basile, G.; Acosta, M.; Scott, G.; Roskelley, C.; Medrano, E. E.; Linskens, M.; Rubelj, I.; Pereira-Smith, O. *Proc. Natl. Acad. Sci. U.S.A.* **1995**, *92*, 9363-9367.
(19) Chatterjee, S. K.; Bhattacharya, M.; Barlow, J. J. *Cancer Res.* **1979**, *39*, 1943-1951.
(20) Peng, L.; Gao, M.; Cai, X.; Zhang, R.; Li, K.; Feng, G.; Tong, A.; Liu, B. *J. Mater. Chem. B* **2015**, *3*, 9168-9172.
(21) Lee, H. W.; Heo, C. H.; Sen, D.; Byun, H.; Kwak, I. H.; Yoon, G.; Kim, H. M. *Anal. Chem.* **2014**, *86*, 10001-10005.
(22) Han, J.; Han, M. S.; Tung, C. *Mol. Biosyst.* **2013**, *9*, 3001-3008.
(23) Kamiya, M.; Asanuma, D.; Kuranaga, E.; Takeishi, A.; Sakabe, M.; Miura, M.; Nagano, T.; Urano, Y. *J Am. Chem. Soc.* **2011**, *133*, 12960-12963.
(24) Wehrman, T. S.; von Degenfeld, G.; Krutzik, P. O.; Nolan, G. P.; Blau, H. M. *Nat. Methods* **2006**, *3*, 295-301.
(25) Asanuma, D.; Sakabe, M.; Kamiya, M.; Yamamoto, K.; Hiratake, J.; Ogawa, M.; Kosaka, N.; Choyke, P. L.; Nagano, T.; Kobayashi, H.; Urano, Y. *Nat. Commun.* **2015**, *6*, 6463.
(26) Yin, J.; Kwon, Y.; Kim, D.; Lee, D.; Kim, G.; Hu, Y.; Ryu, J.; Yoon, J. *J Am. Chem. Soc.* **2014**, *136*, 5351-5358.
(27) Lim, S.; Hong, K.; Kim, D. I.; Kwon, H.; Kim, H. *J Am. Chem. Soc.* **2014**, *136*, 7018-7025.
(28) Guo, Z.; Park, S.; Yoon, J.; Shin, I. *Chem. Soc. Rev.* **2014**, *43*, 16-29.
(29) Yuan, L.; Lin, W.; Zheng, K.; He, L.; Huang, W. *Chem. Soc.*

Rev. **2013**, *42*, 622-661.
(30) Truman, L. K.; Comby, S.; Gunnlaugsson, T. *Angew. Chem. Int. Ed.* **2012**, 51, 9624-962.
(31) Cui, M.; Ono, M.; Watanabe, H.; Kimura, H.; Liu, B.; Saji, H. *J Am. Chem. Soc.* **2014**, *136*, 3388-3394.
(32) McMahon, B. K.; Gunnlaugsson, T. *J Am. Chem. Soc.* **2012**, *134*, 10725-10728.
(33) Niu, L. Y.; Guan, Y. S.; Chen, Y. Z.; Wu, L. Z.; Tung, C. H.; Yang, Q. Z. *J Am. Chem. Soc.* **2012**, *134*, 18928-18931.
(34) Wang, X.; Guo, Z.; Zhu, S.; Tian, H.; Zhu, W. H. *Chem. Commun.* **2014**, *50*, 13525-13528.
(35) Tung, C.; Zeng, Q.; Shah, K.; Kim, D.; Schellingerhout, D.; Weissleder, R. *Cancer Res.* **2004**, *64*, 1579 -1583.
(36) Fan, J.; Hu, M.; Zhan, P.; Peng, X. *Chem. Soc. Rev.* **2013**, *42*, 29-43.
(37) Guo, Z.; Kim, G.; Yoon, J.; Shin, I. *Nat. Protoc.* **2014**, *9*, 1245-1254.
(38) Huang, C.; Ja, T.; Tang, M.; Yin, Q.; Zhu, W.; Zhang, C.; Yang, Y.; Ja, N.; Xu, Y.; Qian, X. *J Am. Chem. Soc.* **2014**, *136*, 14237-14244.
(39) Chen, Y.; Zhu, C.; Yang, Z.; Chen, J.; He, Y.; Jao, Y.; He, W.; Qiu, L.; Cen, J.; Guo, Z. *Angew. Chem. Int. Ed.* **2013**, 52, 1688 -1691.
(40) Yang, Y.; Zhao, Q.; Feng, W.; Li, F. *Chem. Rev.* **2013**, *113*, 192-270.
(41) Guo, Z.; Zhu, W. H.; Tian, H. *Chem. Commun.* **2012**, *48*, 6073-6084.
(42) Wu, X.; Sun, X.; Guo, Z.; Tang, J.; Shen, Y.; James, T. D.; Tian, H.; Zhu, W. H. *J Am. Chem. Soc.* **2014**, *136*, 3579-3588.
(43) Li, M.; Wu, X.; Wang, Y.; Li, Y.; Zhu, W. H.; James, T. D. *Chem. Commun.* **2014**, *50*, 1751-1753.
(44) Sun, W.; Fan, J.; Hu, C.; Cao, J.; Zhang, H.; Xiong, X.; Wang, J.; Cui, S.; Sun, S.; Peng, X. *Chem. Commun.* **2013**, *49*, 3890-3892.
(45) Zheng, Y.; Zhao, M.; Qiao, Q. L.; Liu, H. Y.; Lang, H. J.; Xu, Z. C. *Dyes Pigm.* **2013**, *98*, 367-371.
(46) Zhu, W. H.; Huang, X.; Guo, Z.; Wu, X.; Yu, H.; Tian, H. *Chem. Commun.* **2012**, *48*, 1784-1786.
(47) Rotman, B.; Zderic, J. A.; Edelstein, M. *Proc. Natl. Acad. Sci. U.S.A.* **1963**, *50*, 1-6.
(48) Hamilton, T. C.; Young, R. C.; McKoy, W. M.; Grotzinger, K. R.; Green, J. A.; Chu, E. W.; Whang-Peng, J.; Rogan, A. M.; Green, W.R.; Ozols, R. F. *Cancer Res.* 1983, 43, 5379-5389.
(49) Shukla, H.; Chaplin, M. *Enzyme Microb. Tech.* 1993, 15, 297-299.
(50) Senter, P. D.; Saulnier, M. G.; Schreiber, G. J.; Hirschberg, D. L.; Brown, J. P.; Hellström, I.; Hellström, K. E. *Proc. Natl. Acad. Sci. U.S.A.* **1988**, *85*, 4842-4846.
(51) Senter, P. D.; Springer, C. J. *Adv. Drug Deliver Rev.* **2001**, *53*, 247-264.
(52) Lotan, R.; Raz, A. *Ann. N. Y. Acad. Sci.* **1988**, *551*, 385-398.
(53) Gabius, H. J.; Engelhardt, R.; Cramer, F. *Anticancer Res.* **1986**, *6*, 573-578.

Table of contents (TOC)